Computational Studies on Electron and Proton Transfer in Phenol-Imidazole-Base Triads

SHIHAI YAN,[1] SUNWOO KANG,[1] TOMOYUKI HAYASHI,[2] SHAUL MUKAMEL,[2] JIN YONG LEE[1]
[1]*Department of Chemistry, SungKyunKwan University, Suwon 440-746, Korea*
[2]*Department of Chemistry, University of California at Irvine, Irvine, California 92697-2025*

Received 23 May 2008; Revised 27 February 2009; Accepted 21 April 2009
DOI 10.1002/jcc.21339
Published online in Wiley InterScience (www.interscience.wiley.com).

Abstract: The electron and proton transfer in phenol-imidazole-base systems (base = NH_2^- or OH^-) were investigated by density-functional theory calculations. In particular, the role of bridge imidazole on the electron and proton transfer was discussed in comparison with the phenol-base systems (base = imidazole, H_2O, NH_3, OH^-, and NH_2^-). In the gas phase phenol-imidazole-base system, the hydrogen bonding between the phenol and the imidazole is classified as short strong hydrogen bonding, whereas that between the imidazole and the base is a conventional hydrogen bonding. The *n* value in sp^n hybridization of the oxygen and carbon atoms of the phenolic CO sigma bond was found to be closely related to the CO bond length. From the potential energy surfaces without and with zero point energy correction, it can be concluded that the separated electron and proton transfer mechanism is suitable for the gas-phase phenol-imidazole-base triads, in which the low-barrier hydrogen bond is found and the delocalized phenolic proton can move freely in the single-well potential. For the gas-phase oxidized systems and all of the triads in water solvent, the homogeneous proton-coupled electron transfer mechanism prevails.

 J Comput Chem 00: 000–000, 2009

Key words: proton-coupled electron transfer; low-barrier hydrogen bond; stabilization energy; ionization potential; density-functional theory

Introduction

Proton transfer and electron transfer are fundamental and ubiquitous processes in chemistry and biology. These two processes take place together in some systems to which extensive experimental and theoretical efforts have been devoted.[1–8] According to the way of proton and electron transfer, the process can be classified into three types, hydrogen atom transfer (HAT), proton-coupled electron transfer (PCET) or electron-coupled proton transfer (ECPT), and ET + PT. When an electron and a proton transfer homogeneously to the same terminal at the same time, the process is called HAT.[9–11] On the other hand, when an electron and a proton transfer at the same time but to the different terminals, the process is called PCET or ECPT. Finally, when an electron and a proton transfer separately, the process is called ET + PT. An important example of PCET is the formation of tyrosyl radical by long-range electron transfer coupled deprotonation.[12–14] In photosystem II (PS II), an electron of tyrosine Y_Z transfers to $P680^+$ on oxidation, which is coupled with the proton transfer from tyrosine to the adjacent base, hydrogen-bonded histidine. Simultaneously, it is reported that an electron is transferred from metal cluster to Y_Z and the proton delocalization takes place in a concerted fashion between Y_Z and nearby water.[15–17] The mechanisms of such processes are controversial in some systems, especially regarding the types of electron and proton transfers. For example, in the wild type of *Synechocystis* sp. PCC 6803, one mechanism supports the electron transfer from Mn^{II} to tyrosyl radical (Tyr161) accompanied by H^+ transfer from Mn-OH_2 to His190 through Tyr161, whereas the other mechanism supports H^+ transfer from Mn-OH_2 to Asp61.[8]

As the simplest aryl alcohol, phenol (PhOH) can serve as a prototype for large biological species such as tyrosine residue in proteins. PhOH is versatile for its capability to donate and accept both proton and electron (Scheme 1). PhOH and imidazole (ImH) were previously used as a model system for tyrosine and histidine residues, respectively, to investigate the oxidation of Y_Z in PS II.[18] The hydrogen-bonded PhOH complexes with simple solvent molecules (H_2O and NH_3) were adapted as important models for the investigations of H-bonding, electron transfer, and proton pump in proteins and nucleic acids at the

Additional Supporting Information may be found in the online version of this article.

Correspondence to: J. Y. Lee; e-mail: jinylee@skku.edu

Contract/grant sponsor: Korea Government (MEST); contract/grant numbers: R01-2008-000-10653-0, R01-2007-012-03002-0

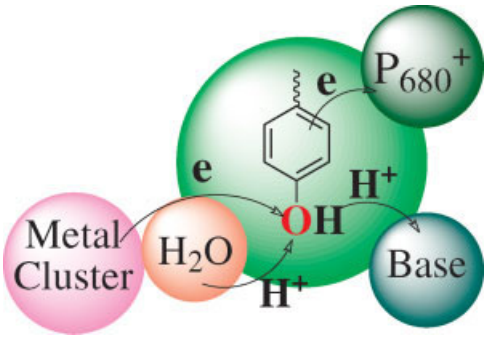

Scheme 1.

molecular level.[19–26] Intramolecular proton transfer is one of the most fundamental chemical processes in acid–base reactions. Adducts organized by PhOH and various base molecules have been explored extensively as prototype for solute and hydrophilic solvent interactions and "solvent-induced excited state proton transfer reaction."[27–31] In particular, the size dependence and the geometrical effects of the energetics and dynamics of proton transfer have been of particular interests. Recently, the substituent effects[32–34] and solvent effects[35,36] on the kinetics of electron transfer reactions of phenoxyl radicals and hydrogen abstraction reactions from PhOHs have been studied. Many experimental works regarding the solvent effect on excited-state proton transfer reaction have been carried out.[37,38] Although the proton transfer mechanism in the $[PhOH\cdots NH_3]^+$ system is intriguing, it is still unclear. Early experiments on this system revealed that there is a high barrier between the double-well potential energy surfaces (PES).[39–44] On the other hand, recent experimental and theoretical results have shown that the proton can transfer to the ammonia moiety facilely and PhO. . .HNH_3^+ is the predominant product.[45–52]

Although it has been proposed that the proton can further transfer to the inner thylakoid through the adjacent base after the phenolic proton is transported to histidine on oxidation, the investigation on the proton transfer between PhOH and base, especially, the proton transfer between histidine mediated phenol and base, is still very scarce. OH^- and NH_2^- are very strong bases and may be harmful for the living organisms; however, it is very interesting to explore the proton transfer depending on the basicity. Therefore, we use the imidazole-mediated phenol and base (OH^- and NH_2^-) triads as model systems to explore the possibility for the proton transfer to the base via imidazole depending on the basicity and reveal the detailed electron and proton transfer mechanism during this process.

Computational Details

The investigated phenol-base dyads and PhOH-ImH-base triads are shown in Figure 1. The well developed density-functional theory (DFT) with the Becke three parameterized Lee–Yang–Parr (B3LYP) exchange correlation functionals has been proven to be successful in describing large free radicals and intermolecular complexes.[53–58] Therefore, we carried out DFT calculations using B3LYP with 6-311++G** basis sets using a suite of Gaussian 03 programs.[59] The vibrational frequency calculations were performed at the same level to confirm the optimized geometries to be local minima or transition states on the PES. The ionization potential (IP) is the energy required to remove an electron from the system. Natural bond orbital (NBO) population analyses[60] are carried out to explore the atomic charge variations during the proton and electron transfer processes. To consider the solvent effect on the energy profile for the proton transfer, the polarizable continuum model (PCM)[61–63] is used within the framework of the self-consistent reaction field (SCRF) theory, which is well-developed and accepted in treating solvent effects of molecular properties.[64–67] Here, the solvent effects are estimated using the water solvent as an example, and the structures in water solvent are fully optimized using the PCM model. The basis set superposition errors (BSSE) for the interaction energies

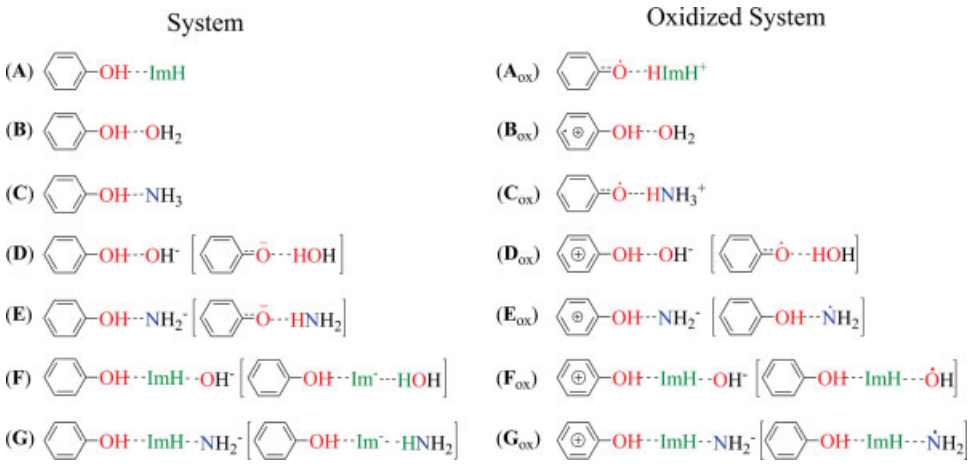

Figure 1. The phenol-base dyads (base = immidazole (ImH), H_2O, NH_3, OH^-, and NH_2^-) and the phenol-immidazole-base triads (base = OH^- and NH_2^-). The sketches in square brackets are the structures obtained after the geometry optimization.

Table 1. Bond Lengths (R_{CO}, R_{OH}, and R_{DA}), Stabilization Energies (ΔE_e and ΔE_0), and Ionization Potentials (IP) of Phenol as well as the Corresponding Dyads and Triads in Gas Phase.

	R_{CO}	R_{OH}	R_{DA}	ΔE_e	ΔE_0	IP		R_{CO}	R_{OH}	R_{DA}	ΔE_e	ΔE_0
PhO	1.270					51.5	PhO	1.253				
PhOH	1.370	0.963				192.2	$PhOH^+$	1.310	0.972			
A	1.355	0.985	2.826	−9.7	−8.4	158.0	$\mathbf{A}_{ox}$	1.263	1.625	2.650	−44.0	−42.6
B	1.362	0.972	2.849	−7.2	−5.2	178.4	$\mathbf{B}_{ox}$	1.298	1.013	2.594	−21.0	−19.0
C	1.356	0.984	2.853	−9.0	−7.0	170.8	$\mathbf{C}_{ox}$	1.268	1.501	2.577	−30.6	−28.4
D	1.284	1.662	2.658	−58.6	−57.6	61.5	$\mathbf{D}_{ox}$	1.258	1.907	2.845	−190.0	−188.3
E	1.278	1.911	2.933	−67.0	−64.8	56.4	$\mathbf{E}_{ox}$	1.359	0.976	2.912	−183.8	−181.7
							$\mathbf{E}_{ox}{}^T$	1.331	1.107	2.437	−179.9	−180.1
							$\mathbf{E}_{ox}{}'$	1.256	2.234	3.182	−203.7	−200.6

	R_{CO}	R_{OH}	R^1_{DA}	R^2_{DA}	ΔE_e	ΔE_0	IP		R_{CO}	R_{OH}	R^1_{DA}	R^2_{DA}	ΔE_e	ΔE_0
F	1.332	1.054	2.598	2.788	−80.1	−78.5	104.4	$\mathbf{F}_{ox}$	1.335	1.011	2.692	2.826	−168.4	−166.3
$\mathbf{F}^T$	1.313	1.231	2.490	2.808	−79.4	−80.0	104.8	$\mathbf{F}_{ox}{}^T$	1.302	1.184	2.484	2.621	−166.2	−167.3
F′	1.297	1.463	2.569	2.827	−79.9	−78.6	75.0	$\mathbf{F}_{ox}{}'$	1.256	1.918	2.937	2.892	−198.3	−195.8
G	1.330	1.068	2.578	3.109	−89.2	−86.4	87.7	$\mathbf{G}_{ox}$	1.354	0.989	2.801	3.038	−194.0	−190.8
$\mathbf{G}^T$	1.316	1.194	2.493	3.126	−88.8	−88.0	98.1	$\mathbf{G}_{ox}{}^T$	1.291	1.418	2.535	2.649	−182.3	−182.1
G′	1.295	1.501	2.591	3.154	−89.9	−87.1	72.6	$\mathbf{G}_{ox}{}'$	1.256	1.932	2.950	3.158	−210.7	−206.6

R_{CO}, R_{OH}, and R_{DA} denote the C—O, O—H bond length of phenol, and the distance between H-bond donor (D = O or N) and acceptor (A = N or O), their units are in angstrom (Å). ΔE_e, ΔE_0, and IP refer to the stabilization energy, zero-point energy corrected stabilization energy, and the ionization potential, respectively. They are all in kcal/mol. $\mathbf{X}'$ denotes the proton transferred state from the phenol to the imidazole bridge of **X**. $\mathbf{X}^T$ denotes the transition state between **X** and $\mathbf{X}'$. $\mathbf{X}^T_{ox}$ and $\mathbf{X}'_{ox}$ represent the oxidized species corresponding to $\mathbf{X}^T$ and $\mathbf{X}'$. R^1_{DA} and R^2_{DA} denote the H-bond length between the phenolic oxygen and the nitrogen atom of the imidazole bridge and the distance between the nitrogen of the bridging imidazole and the oxygen/nitrogen of OH^-/NH_2^-. IP of **X** was obtained by $IP(\mathbf{X}) = E(\mathbf{X}^+) - E(\mathbf{X})$; where $E(\mathbf{X}^+)$ and $E(\mathbf{X})$ are the energies of the optimized $\mathbf{X}^+$ and **X**, respectively.

were corrected by the counter-poise method without further optimization at the non-BSSE optimized structures.

Results and Discussions

The variations of principal structural parameters of phenol adducts are listed in Table 1. Table 2 presents the corresponding parameters obtained in water solvent. For the gas-phase dyads, PhOH···ImH (**A**), PhOH···OH_2 (**B**), and PhOH···NH_3 (**C**), it was found that the hydroxy proton of PhOH did not transfer spontaneously, while it transferred to the neighbor for PhOH···OH^- (**D**) and PhOH···NH_2^- (**E**) becoming PhO^-···OH_2 and PhO^-···NH_3, respectively, as recognized by the OH bond length (1.662 and 1.911 Å for **D** and **E**, respectively) of PhOH. The similar phenomena were also observed in water solvent. Because of the hydroxy proton transfer between PhOH and charged species, the interaction energies for the charged bases (OH^- and NH_2^-) become much larger than the neutral bases. In Table 1, the oxidized species are denoted by subscript "ox", for example, $\mathbf{A}_{ox}$ for the oxidized species of **A**. On oxidation (one electron removal), no matter in gas phase or in water solvent, the hydroxy proton of PhOH transferred spontaneously to the counter bases (ImH, NH_3, and OH^-) in the dyads except PhOH...OH_2 as noted in Tables 1 and 2. Compared with the results obtained at CASSCF(9E10M)/6-31++G(d,p) level for PhOH and PhOH-NH_3, our calculations are reliable.[68] Furthermore, our results are also consistent with the previous experimental and theoretical explorations.[18,32–34,69] It is interesting to find that there are two stable states, proton transferred and nontransferred state, for $\mathbf{E}_{ox}$. From the geometry parameters optimized in gas phase (Table 1) and water solvent (Table 2), the general conclusion can be drawn that the CO and OH bonds length of phenol (R_{CO} and R_{OH}) increase in water solvent. The distances between H-bond donor and acceptor (R_{DA}) of A, B, and C shorten in water solvent.

The corrections of the BSSE on the stabilization energy may improve the energy quantities, while the relative regularity may not be altered because the contribution from the BSSE correction is significantly smaller when compared with the corresponding uncorrected values. The BSSE values for the dyads are calculated and represented in Supporting Information. These values are almost less than 1 kcal/mol. Furthermore, for comparison with the triads, we did not give the BSSE corrected stabilization energy in the text.

Here, we are interested in the electron and proton transfer mechanism between PhOH and strong bases, NH_2^- and OH^-, under the influence of the ImH bridge. The detailed systems are shown in Figure 1. Two different states are observed for each ImH bridged system for both OH^- and NH_2^-. One state is that a proton is transferred from the ImH to OH^-/NH_2^- (**F**/**G**). The other state is that one proton is transferred from PhOH to ImH with another proton transferred from the ImH to OH^-/NH_2^- at the same time ($\mathbf{F}'/\mathbf{G}'$). The transition state between **F** and $\mathbf{F}'$ is denoted as $\mathbf{F}^T$. Similarly, $\mathbf{G}^T$ denotes the transition state between **G** and $\mathbf{G}'$. $\mathbf{F}_{ox}{}^T$ and $\mathbf{G}_{ox}{}^T$ denote the transition states for the cor-

Table 2. Bond Lengths (R_{CO}, R_{OH}, and R_{DA}), Stabilization Energies (ΔE_e and ΔE_0), and Ionization Potentials (IP) of Phenol as well as the Corresponding Dyads and Triads in Water Solvent.

	R_{CO}	R_{OH}	R_{DA}		ΔE_e	ΔE_0	IP		R_{CO}	R_{OH}	R_{DA}		ΔE_e	ΔE_0
PhO^-	1.298						103.6	PhO	1.260					
PhOH	1.368	0.983					138.4	$PhOH^+$	1.305	1.005				
A	1.358	1.003	2.722		−3.5	−1.9	119.1	$\mathbf{A}_{ox}$	1.264	1.738	2.773		−23.1	−21.2
B	1.363	0.984	2.732		−2.2	0.23	134.7	$\mathbf{B}_{ox}$	1.295	1.039	2.520		−5.7	−3.5
C	1.357	1.005	2.735		−4.8	−2.4	123.7	$\mathbf{C}_{ox}$	1.265	1.685	2.730		−20.7	−17.1
D	1.307	1.664	2.663		−20.7	−18.7	106.8	$\mathbf{D}_{ox}$	1.262	1.869	2.843		−52.7	−50.3
E	1.299	2.011	3.037		−37.6	−34.4	120.5	$\boldsymbol{E}_{ox}$	1.362	0.991	2.783		−55.1	−52.3
								$\boldsymbol{E}_{ox}^{T}$	1.340	1.145	2.429		−49.2	−49.1
							103.9	$\boldsymbol{E}_{ox}'$	1.261	2.251	3.270		−73.5	−68.9
	R_{CO}	R_{OH}	R_{DA}^1	R_{DA}^2	ΔE_e	ΔE_0	IP		R_{CO}	R_{OH}	R_{DA}^1	R_{DA}^2	ΔE_e	ΔE_0
F	1.352	1.037	2.623	2.772	−24.6	−21.9	140.2	$\mathbf{F}_{ox}$	1.358	1.004	2.716	2.995	−23.1	−20.1
$\mathbf{F}^T$	1.330	1.253	2.487	2.795	−21.4	−21.1	124.3	$\mathbf{F}_{ox}^{T}$	1.303	1.190	2.489	2.635	−15.2	−15.2
F′	1.310	1.596	2.659	2.818	−25.7	−22.9	108.4	$\mathbf{F}_{ox}'$	1.263	1.863	2.885	2.833	−56.6	−53.0
G	1.351	1.044	2.608	3.217	−41.2	−37.4	121.7	$\mathbf{G}_{ox}$	1.358	1.006	2.711	2.940	−57.9	−54.0
$\mathbf{G}^T$	1.349	1.349	2.606	3.193	−34.9	−33.7	145.4	$\mathbf{G}_{ox}^{T}$	1.299	1.332	2.559	2.640	−39.8	−40.3
G′	1.309	1.614	2.673	3.260	−42.2	−38.1	106.8	$\mathbf{G}_{ox}'$	1.262	1.876	2.897	3.271	−74.5	−69.7

R_{CO}, R_{OH}, and R_{DA} denote the C—O, O—H bond length of phenol, and the distance between H-bond donor (D = O or N) and acceptor (A = N or O), their units are Å. ΔE_e, ΔE_0, and IP refer to the stabilization energy, zero-point energy corrected stabilization energy, and the ionization potential, respectively. They are all in kcal/mol. **X′** denotes the proton transferred state from the phenol to the imidazole bridge of **X**. $\mathbf{X}^T$ denotes the transition state between **X** and **X′**. X_{ox}^T and X_{ox}' represent the oxidized species corresponding to $\mathbf{X}^T$ and **X′**. R_{DA}^1 and R_{DA}^2 denote the H-bond length between the phenolic oxygen and the nitrogen atom of the imidazole bridge and the distance between the nitrogen of the bridging imidazole and the oxygen/nitrogen of OH^-/NH_2^-.

responding oxidized species. The CO bond length of PhOH, R_{CO}, shortens to an extent on oxidation for all selected systems except **F** and **G** (Tables 1 and 2). This variation reflects the decrease of phenolate characteristic and the enhancement of oxidized neutral phenoxy radical property. The R_{CO} bonds in water solvent are longer than those in gas phase.

In these gas-phase triads, the hydrogen bond distances between PhOH and ImH are very short as noted in R_{DA}^1 values. Before PT, the O···N distance of **F**/**G** is 2.598/2.578 Å, and it changes to 2.569/2.591 Å after PT. Based on the previously suggested concept of short strong hydrogen bond (SSHB),[70–78] such bonds belong to SSHB category. In our previous study, the acid–base dual role was addressed in KSI enzymatic catalysis through SSHB.[77,78] SSHB has been suggested in enzymatic catalytic mechanism, where the proton affinities of the two anions are matched when the single-well minima occur after the zero-point vibrational energy (ZPE) correction.[79] Our results support this proposition as noted in the proton affinities of the phenolate and the imidazole anions. We will discuss SSHB later in more detail.

Figure 2 represents the sp^n hybridization character of C and O atoms of the phenolic CO sigma bond versus CO bond lengths for all the systems investigated in gas phase. It is clearly shown in Figure 2a, as the CO bond length increases, the *n* value of the sp^n hybridization increases, that is, the *p*-character of the CO sigma bond increases, which is consistent with the previous studies.[80,81] Furthermore, at the limit of the longest CO bond length, the hybridization character of the CO sigma orbital localized at C and O is approaching to sp^3 and sp^2, respectively. The CO sigma orbital of the PhOH is the linear combination of the two localized orbitals at C and O atoms. In Figure 2b, it is clearly seen that the *n* values of the sp^n hybridization of both C and O atoms decrease on oxidation. This is because the benzene structure of the PhOH changes to the quinoidal structure by an extent on oxidation, and the CO bond length is shortened. This tendency is reversed when **F** and **G** are oxidized. The CO bond lengths for $\mathbf{F}/\mathbf{F}_{ox}$ and $\mathbf{G}/\mathbf{G}_{ox}$ are 1.332/1.335 Å and 1.330/1.354 Å, respectively, whereas for $\mathbf{F}'/\mathbf{F}_{ox}'$ and $\mathbf{G}'/\mathbf{G}_{ox}'$ are 1.297/1.256 Å and 1.295/1.256 Å, respectively. The *n* values of the sp^n hybridization character of C and O atoms are 2.72/2.83/ 2.70/ 2.91/ 2.41/2.34/ 2.39/2.34 and 1.84/1.85/ 1.83/1.90/ 1.73/1.57/ 1.72/1.58 for $\mathbf{F}/\mathbf{F}_{ox}$/ $\mathbf{G}/\mathbf{G}_{ox}$/ $\mathbf{F}'/\mathbf{F}_{ox}'$ / $\mathbf{G}'/\mathbf{G}_{ox}'$, respectively. Generally speaking, the *s*-character of CO sigma bond increases and the *p*-character decreases as the CO bond length decreases.

In both gas phase and water solvent, regardless of the proton being transferred or not, the OH bond of PhOH, R_{OH}, lengthens on oxidation except those in **F** and **G**. Although most of the R_{OH} increase when oxidized, the underlying mechanisms are quite different for the complexes generated by PhOH with small solvent molecules (NH_3 and H_2O) and the corresponding conjugate bases (NH_2^- and OH^-). For the oxidation of dimeric complexes, **A**, **B**, and **C**, an electron is detached from the PhOH fragment because the IP of the PhOH[82,83] (192.2 kcal/mol) is smaller than that of the ImH (201.6 kcal/mol), NH_3 (234.1 kcal/mol), and H_2O (290.7 kcal/mol). Therefore, on oxidation, the OH bond strength of the PhOH decreases. On the other hand, for the complexes **D** and **E**, an electron seems to be removed from the bases because of their smaller IPs than the PhOH

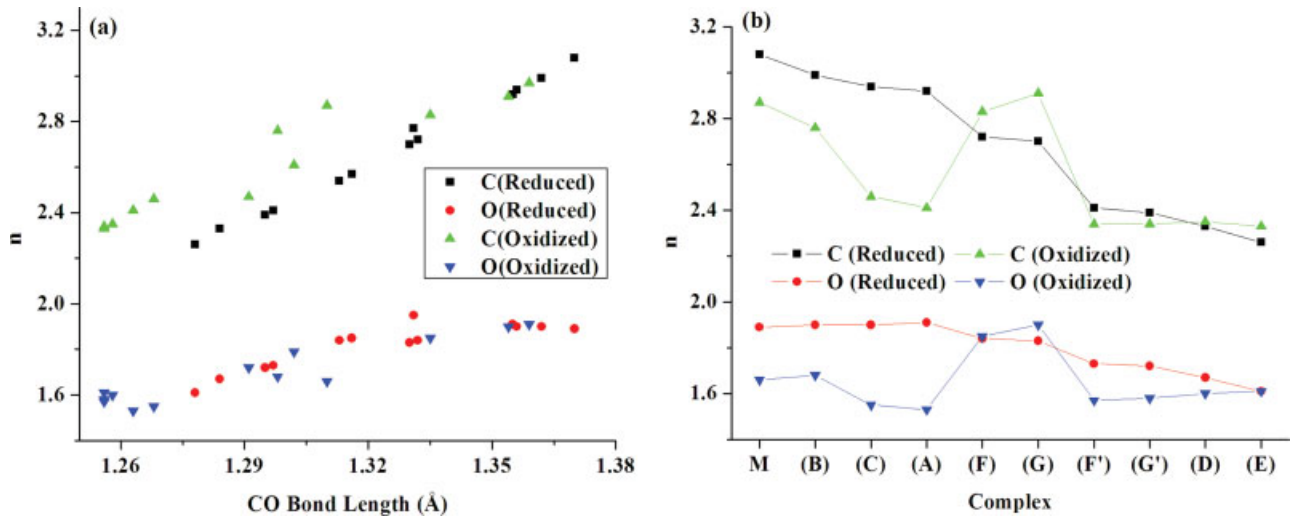

Figure 2. (a) The sp^n hybrid character of the phenolic CO sigma bond versus CO bond length; (b) The sp^n hybrid character of the phenolic CO sigma bond in different systems. M denotes the phenol monomer.

(Table 1 and Supporting Information). However, the phenolic proton transfers to NH_2^- and OH^- after the geometry optimization, and the excess electron is localized on the phenoxy anion fragment. Therefore, when oxidized, an electron should be detached from the phenoxy anion moiety and the electron density populated at the phenoxy moiety reduces. The nonproton transferred conformation ($\mathbf{E}_{ox}$) also exists for the oxidized PhOH complex with NH_2^-. In addition, the spin density populations reveal that an electron is localized on the $^{\bullet}NH_2$ fragment before the phenolic proton transfer, whereas the phenoxy radical with singly occupied orbital is generated after the proton transfer as seen in Supporting Information. Furthermore, the spin density populated on the phenolic proton is approaching to zero during the proton transfer process. Therefore, the PCET mechanism can be established for the oxidation process of **E**, which finally gives the product composed of the neutral phenoxy radical and NH_3.

For the triads, **F**/**F**′ and **G**/**G**′, one proton transfers to the OH^- and NH_2^-, and the hydroxy proton of the PhOH may transfer to the ImH bridge or may not. Thus, there exists a double well PES along the proton transfer coordinates between **F**(**G**) and **F**′(**G**′). It was reported that the central maximum on the proton transfer PES may fall below the ground state on the ZPE correction when the hydrogen bond is sufficiently short, as leading to a delocalized proton and the double-well metabolizing into a single-well after inclusion of ZPE.[79,84] Such SSHB is also named as the low-barrier hydrogen bond (LBHB).[85–88] The important criterion for LBHB is that the proton affinities (PA, the energy difference of phenol/imidazole and phenolate/deprotonated ImH) of the two anions which share the proton should be almost equal to each other.[79] Here, the PAs of the phenolate and the deprotonated ImH anion are 345.2 and 348.3 kcal/mol in gas phase, 295.5 and 298.7 kcal/mol in water solvent, respectively. The solvation energy calculated by SCRF is based on the perturbation on electron density of the appearance of a solvent. The proton has no electron density, thus no solvation energy. Thus, the proton affinities of PhO^- and Im^- in water are obtained with the same method as in gas phase, subtracting the energies of PhO^- and Im^- from those of PhOH and ImH, separately. Our results are in well accordance with this requirement. After the two separate steps, the electron is transferred from OH^-/NH_2^- base to the PhOH, and the phenolic proton is delivered to the base by way of the bridging ImH. The electron and proton transfer mechanism for these anion triads is different from the HAT mechanism for chromophore-to-solvent proton-transfer reaction.[52]

The corresponding oxidized complex can be taken as the interaction of $PhOH^+$ and OH^-/NH_2^- mediated by ImH fragment. During the reorganization, the electron transfers from OH^-/NH_2^- base to $PhOH^+$ cation radical through the ImH bridge. Here, no spontaneous PT is found. The bond lengths of R^l_{DA} for nonproton transferred triads, $\mathbf{F}_{ox}$ and $\mathbf{G}_{ox}$, are 2.692 and 2.801 Å in gas phase, 2.716 and 2.711 Å in water solvent, respectively. The NBO analysis reveals that three fragments are all electroneutral. The spin density represented in Table 3 manifests that the single electron is located on the terminal base fragment. For the proton transferred conformation, the R^l_{DA} distance of $\mathbf{F}'_{ox}$/$\mathbf{G}'_{ox}$ increases distinctly up to 2.937/2.950 Å in gas phase and 2.885/2.897 in water solvent. The spin density analysis demonstrates that the single electron is distributed on phenoxy radical. This indicates that one electron is transferred from the PhOH to the base radical along with the concerted protons transfer.

To distinguish the electron and proton transfer mechanism, we explored the NBO charges and the spin density distributions over all the fragments at the transition state. For gas-phase F^T_{ox}, the NBO charges on PhOH, ImH, and OH fragments are 0.22, 0.15, and −0.37, respectively, whereas the unpaired spin populations are 0.47, 0.00, and 0.54, respectively. It is obvious that the electron is transported to OH radical although the proton is not transferred to ImH fragment. For gas-phase G^T_{ox}, the NBO

Table 3. Spin Density Populations of Oxidized Triads in Gas Phase and Water Solvent.

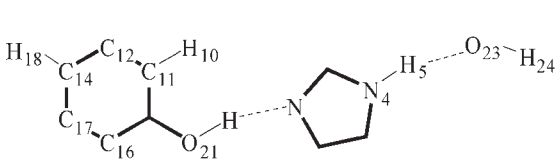

Atomic Numbering for F_{ox}, $F_{ox}{}^{T}$, and F_{ox}'

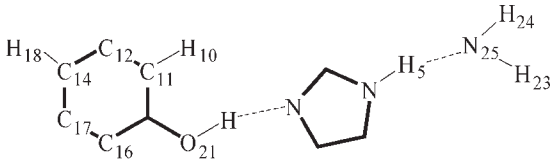

Atomic Numbering for G_{ox}, $G_{ox}{}^{T}$, and G_{ox}'

		N_4	H_5	H_{10}	C_{11}	C_{12}	C_{14}	C_{16}	C_{17}	H_{18}	O_{21}	O_{23}	H_{24}
Gas	$\mathbf{F}_{ox}$	0.012	−0.016	−0.003	0.052	−0.029	0.103	0.037	−0.025	−0.005	0.068	0.786	−0.018
	$\mathbf{F}_{ox}{}^{T}$	0.006	−0.014	−0.008	0.127	−0.067	0.203	0.091	−0.061	−0.011	0.163	0.554	−0.015
	$\mathbf{F}_{ox}'$	0.000	0.000	−0.019	0.302	−0.164	0.430	0.274	−0.155	−0.025	0.393	0.000	0.000
Water	$\mathbf{F}_{ox}$	0.014	−0.021	0.000	0.000	0.000	0.000	0.000	0.000	0.000	0.000	1.033	−0.026
	$\mathbf{F}_{ox}{}^{T}$	0.000	0.000	−0.015	0.232	−0.124	0.435	0.192	−0.129	−0.022	0.312	0.000	0.000
	$\mathbf{F}_{ox}'$	0.000	0.000	−0.018	0.296	−0.158	0.437	0.240	−0.146	−0.023	0.364	0.000	0.000
		H_5	H_{10}	C_{11}	C_{12}	C_{14}	C_{16}	C_{17}	H_{18}	O_{21}	H_{23}	H_{24}	N_{25}
Gas	$\mathbf{G}_{ox}$	−0.028	0.000	0.000	0.000	0.000	0.000	0.000	0.000	0.000	−0.032	−0.033	1.082
	$\mathbf{G}_{ox}{}^{T}$	−0.021	−0.007	0.123	−0.063	0.177	0.094	−0.060	−0.010	0.163	−0.020	−0.020	0.642
	$\mathbf{G}_{ox}'$	0.000	−0.020	0.306	−0.165	0.429	0.273	−0.155	−0.025	0.397	0.000	0.000	0.000
Water	$\mathbf{G}_{ox}$	−0.032	0.000	0.000	0.000	0.000	0.000	0.000	0.000	0.000	−0.033	−0.032	1.086
	$\mathbf{G}_{ox}{}^{T}$	−0.034	0.000	0.000	0.000	0.000	0.000	0.000	0.000	0.000	−0.034	−0.038	1.105
	$\mathbf{G}_{ox}'$	0.000	−0.018	0.296	−0.158	0.437	0.242	−0.146	−0.023	0.364	0.000	0.000	0.000

charges distributed on PhO, HImH, and NH_2 fragments are −0.42, 0.68, and −0.26, respectively. On the other hand, the unpaired spin populations on PhO, HImH, and NH_2 fragments are 0.42, −0.03, and 0.60, respectively. The positive charge located on HImH fragment is due to the transferred phenolic proton, whereas the positive spin densities on PhO and NH_2 radicals are due to the electron transfer from the PhOH to $^{\bullet}NH_2$ radical. Consequently, the electron and the proton transfer in oxidized triads are asynchronous and the mechanism can be classified as the homogenous PCET rather than HAT. In water solvent, the proton and electron transfer mechanism is the same.

As we have the knowledge about the geometry structures, it is easy to understand why the R(OH···N) distances in **F/G** are shorter than those in oxidized $\mathbf{F}_{ox}/\mathbf{G}_{ox}$ triads. For the former anionic systems, the phenolic proton is shared by two anions and the SSHB is generated in gas phase. The following investigations on proton transfer PES also support our proposition about the LBHB. While for the oxidized triads, the typical hydrogen bond is formed between PhOH and ImH groups with the electrostatic interaction. Also we can conclude that the electron effect on these systems is significant. It can be seen from Table 1 that the stability is enhanced significantly on oxidation. Generally, the stability of the ImH mediated triads is higher when compared with the phenol-base dyads. No matter dyads or triads, the binding of the PhOH with NH_3/NH_2^-, is stronger than that with H_2O/OH^-. Furthermore, the proton transfer significantly enhances the stability of the oxidized triads. In other words, F'_{ox} and G'_{ox} are more stable when compared with $\mathbf{F}_{ox}$ and $\mathbf{G}_{ox}$. However, the energy change caused by the pure phenolic proton transfer is not obvious, as can be observed from the proton nontransferred states of **F** and **G** and the proton transferred states of **F′** and **G′**. This phenomenon may be contributed predominantly to the formation of LBHB. These points are all illustrated in the left column of Figure 3. The corresponding PESs with the consideration of solvent effect are represented in the right column of Figure 3. Compared with the PESs obtained in gas phase, the energy barriers for proton transfer reaction in water solvent for both reduced and oxidized states are all increased. As indicated, the hydrogen bonds formed in gas phase are stronger than those formed in water solvent.

The ZPE corrected stabilization energy, ΔE_0, demonstrates that the proton transferred conformation is more stable than the phenolic proton nontransferred geometry, especially, for the oxidized systems. $\mathbf{F}'_{ox}$ and $\mathbf{G}'_{ox}$ are more stable than $\mathbf{F}_{ox}$ and $\mathbf{G}_{ox}$ by about 30 and 16 kcal/mol in gas phase, 33 and 16 in water solvent, respectively. Connected with the proton transfer mechanism, in gas phase, the following intriguing phenomenon can be found: the double-well PES of the anionic **F/G** triad turns into the single-well PES after the ZPE correction, as leads to the typical LBHB. The central maximum disappears and the barrier becomes negative. Therefore, the vibrational ground state of the proton is higher than the activation barrier for the proton transfer process. The transfer mechanism is PCET when the transition state is higher in energy after inclusion of ZPE than the proton transferred conformation. On the other hand, the mechanism is separated ET and PT when the energy of the transition state is

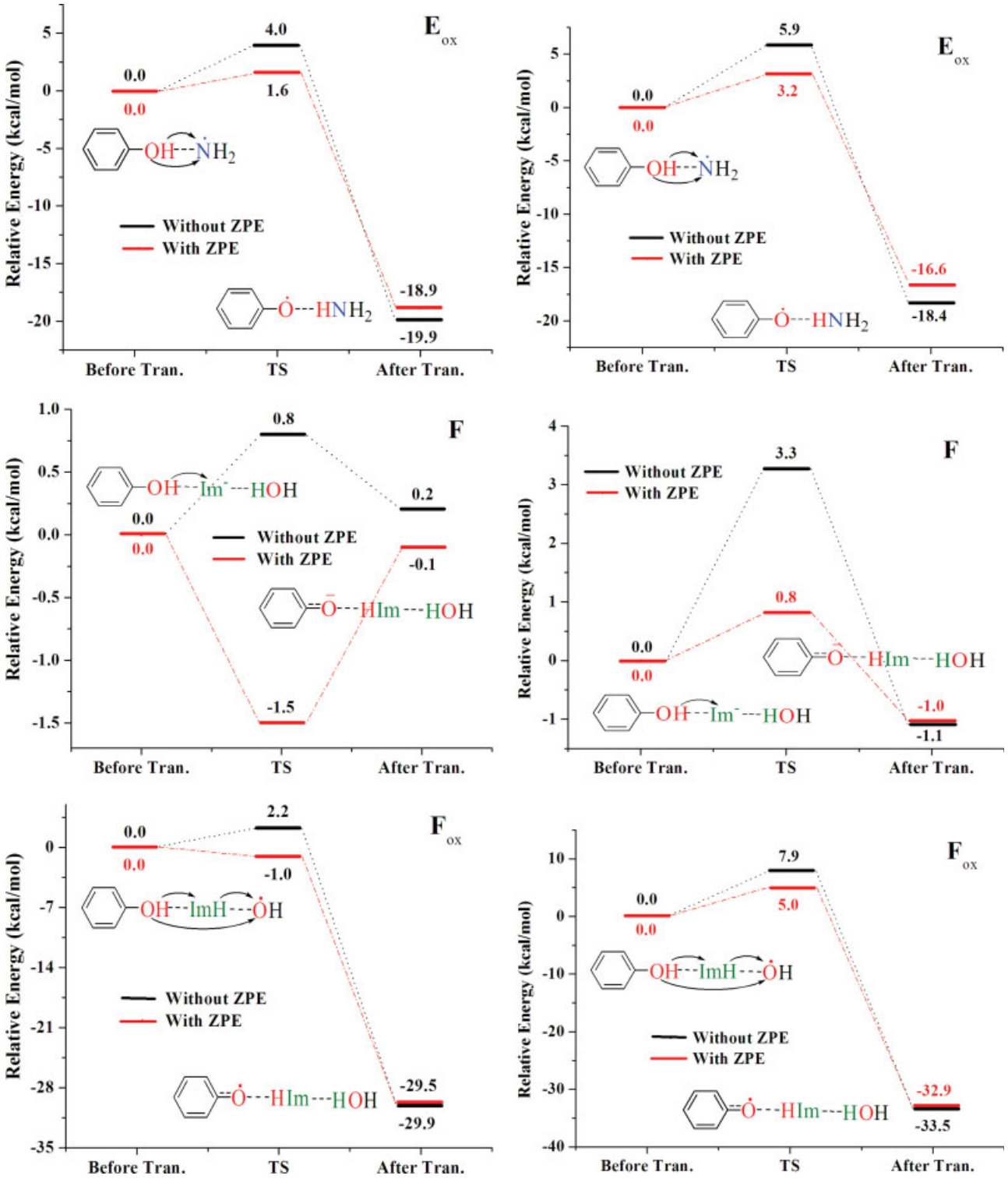

Figure 3. Potential energy surfaces in gas phase (left) and water solvent (right) obtained at B3LYP/6-311++G(d,p) level. The energies before the phenolic proton transfer were taken as references (0). [Color figure can be viewed in the online issue, which is available at www.interscience.wiley.com.]

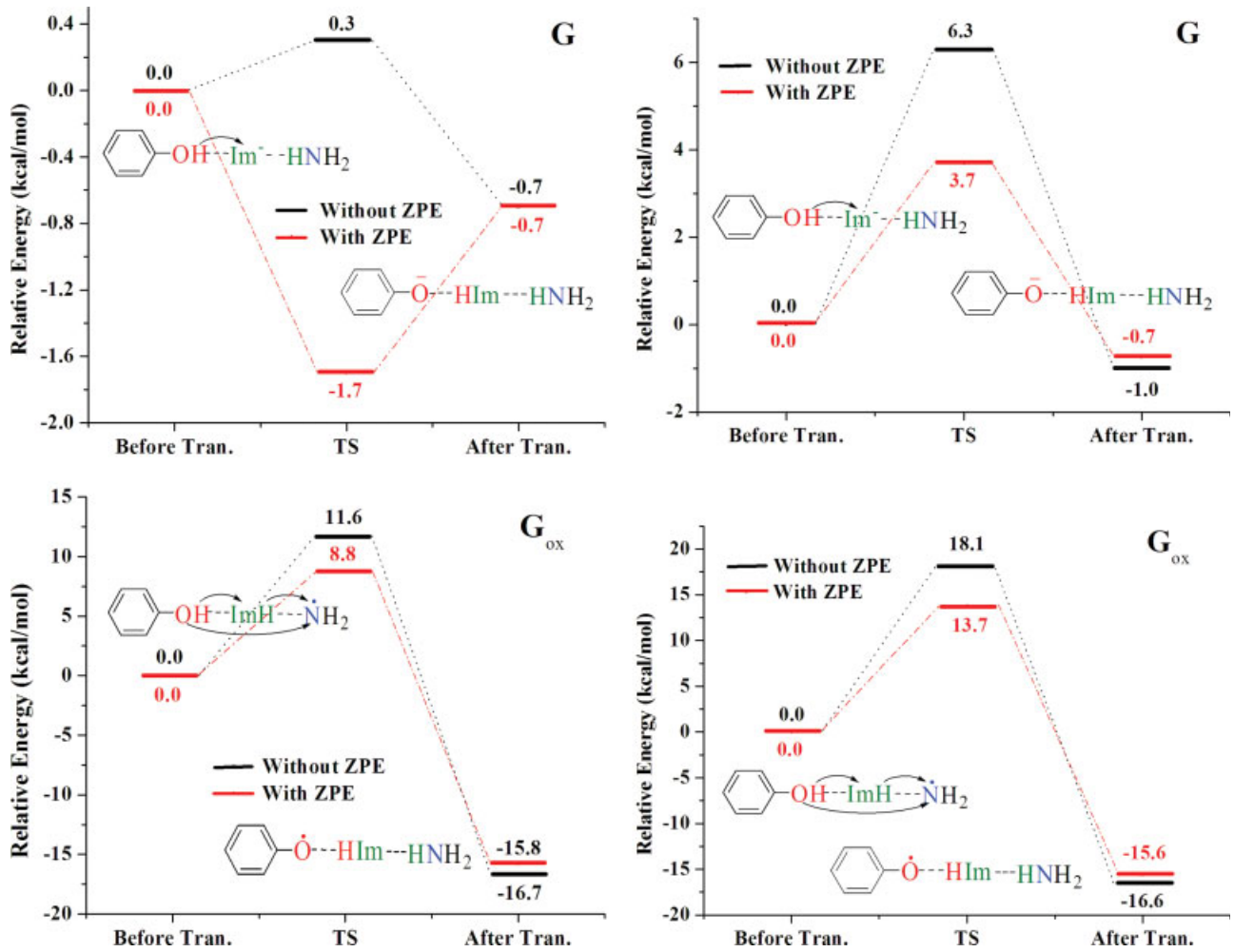

Figure 3. (Continued)

lower than the corresponding reactant and product. For the latter case, the phenolic proton carries the characteristic of LBHB, and the proton is allowed to move freely between the two anions in a barrierless effective potential well.[81] In water solvent, the stability of these triads decrease distinctly (Tables 1 and 2), as should attributed to the weakening of the hydrogen bond strength. The PCET mechanism is suitable for all the triads in water solvent. It is very interesting to find that the electron transfer and proton transfer mechanism can be different in gas phase and water solvent. In both gas phase and water solvent, the proton-transfer energy barriers of the oxidized triads are higher than those of **F** and **G**.

In gas phase, the IPs for **D** and **E** are much lower than the other dyads (Table 1), whereas, in water solvent, the IPs of **D** and **E** are almost equal to those of **A**, **B**, and **C** (Table 2). This demonstrates that the excess electron binds more tightly with the systems in water solvent. For **D** and **E**, the PhOH has some phenolate characteristics, which are reflected by their IP values. The IP values for gas-phase phenolate, **D**, and **E**, are 51.5, 61.5, and 56.4 kcal/mol, respectively. In water solvent, the corresponding values are 103.6, 106.8, and 103.9 kcal/mol, respectively. The IPs collected in Tables 1 and 2 indicate that the combination with small solvent molecules (water and ammonia) or simple bases (OH^- and NH_2^-) lowers the IP value of PhOH in different degrees. Thus, the system can be more easily oxidized after binding with solvent molecules or bases. Furthermore, the complex generated with ammonia and NH_2^- base is easier to be oxidized compared with that formed with water and OH^- base. The IP values of **A**, **F**, and **G** reveal that the system can be oxidized by electron detachment more easily in the presence of bases in close proximity. Furthermore, the IP value can be reduced distinctly by PT. Thus, it is easier to be oxidized on electron detachment for the proton transferred conformations.

Conclusions

Our investigation reveals that the existence of the base assists the phenolic proton transfer. It is found that as the CO bond length increases, the *p*-character of the phenolic CO sigma bond increases, which is consistent with the simple extreme cases of sp^2 hybridization for C=O and sp^3 hybridization of C—O.

Single-well effective potential is established for the dyad generated by the phenol cation radical and OH^- base. PCET mechanism is suitable for the double-well of PhOH-NH_2 complex. In gas phase, the separated ET and PT mechanism is suitable for the ImH mediated PhOH and base triads, where the LBHB exists between the PhOH and the ImH groups. For the oxidized systems, the homogeneous PCET mechanism is determined based on the electronic structures, NBO charges, and spin densities. In water solvent, only the PCET mechanism is observed. The polar water solvent increases the energy barrier for the proton transfer. In both gas phase and water solvent, the energy barrier and the IP indicate that the proton transfer occurs before the electron detachment. Although our analyses are based on the theoretical results, the useful information can be provided to the experimentalists who dedicate to the mechanism exploration and environment optimization, especially for the photosystems.

References

1. Cukier, R. I.; Nocera, D. G. Annu Rev Phys Chem 1998, 49, 337.
2. Hammes-Schiffer, S. Chem Phys Chem 2002, 3, 33.
3. Stubbe, J.; Nocera, D. G.; Yee, C. S.; Chang, M. C. Y. Chem Rev 2003, 103, 2167.
4. Chang, C. J.; Chang, M. C. Y.; Damrauer, N. H.; Nocera, D. G. Biochim Biophys Acta 2004, 1655, 13.
5. McEvoy, J. P.; Brudvig, G. W. Phys Chem Chem Phys 2004, 6, 4754.
6. Rhile, I. J.; Mayer, J. M. J Am Chem Soc 2004, 126, 12718.
7. Costentin, C.; Robert, M.; Savéant, J.-M. J Am Chem Soc 2007, 129, 5870.
8. Meyer, T. J.; Huynh, M. H. V.; Thorp, H. H. Angew Chem Int Ed 2007, 46, 5284; and references therein.
9. Mayer, J. M. Annu Rev Phys Chem 2004, 55, 363.
10. Mayer, J. M.; Rhile, I. J. Biochim Biophys Acta 2004, 1655, 51.
11. Chen, X.; Bu, Y. J Am Chem Soc 2007, 129, 9713.
12. Stubbe, J.; van der Donk, W. A. Chem Rev 1998, 98, 705.
13. Pesavento, R. P.; van der Donk, W. A. Adv Protein Chem 2001, 58, 317.
14. Reece, S. Y.; Hodgkiss, J. M.; Stubbe, J.; Nocera, D. G. Phil Trans R Soc B 2006, 361, 1351.
15. Faller, P.; Goussias, C.; Rutherford, A. W.; Un, S. Proc Natl Acad Sci USA 2003, 100, 8732.
16. Diner, B. A.; Britt, R. D. In Advances in Photosynthesis and Respiration 22; Wydrzynski, T. J.; Satoh, K., Eds.; Springer: Dordrecht, The Netherlands, 2005; p 207.
17. McEvoy, J. P.; Brudvig, G. W. Chem Rev 2006, 106, 4455; and references therein.
18. O'Malley, P. J. J Am Chem Soc 1998, 120, 11732.
19. Feller, D.; Feyereisen, M. J Comput Chem 1993, 14, 1027.
20. Sato, S.; Mikami, N. J Phys Chem 1996, 100, 4765.
21. Sawamura, T.; Fujii, A.; Sato, S.; Ebata, T.; Mikami, N. J Phys Chem 1996, 100, 8131.
22. Re, S.; Osamura, Y. J Phys Chem A 1998, 102, 3798.
23. Pino, G.; Grégoire, G.; Dedonder-Lardeux, C.; Jouvet, C.; Martrenchard, S. Solgadi, D. Phys Chem Chem Phys 2000, 2, 893.
24. Guedes, R. C.; Cabral, B. J. C.; Simões, J. A. M.; Diogo, H. P. J Phys Chem A 2000, 104, 6062.
25. Grégoire, G.; Dedonder-Lardeux, C.; Jouvet, C.; Martrenchard, S. Solgadi, D. J Phys Chem A 2001, 105, 5971.
26. Sobolewski, A. L.; Domcke, W. J Phys Chem A 2001, 105, 9275.
27. Cukier, R. I.; Morillo, M. J Chem Phys 1990, 91, 857.
28. Morillo, M.; Cukier, R. I. J Chem Phys 1990, 92, 4833.
29. Borgis, D.; Hynes, J. T. J Chem Phys 1991, 94, 3619.
30. Syage, J. A. J Phys Chem 1993, 97, 12523.
31. Syage, J. A. Faraday Discuss 1994, 97, 401.
32. Jonsson, M.; Lind, J.; Reitberger, T.; Eriksen, T. E.; Merényi, G. J Phys Chem 1993, 97, 8229.
33. Jin, F.; Leitich, J.; von Sonnatag, C. J Chem Soc Perkin Trans 1993, 2, 1583.
34. Brinck, T.; Haeberlein, M.; Jonsson, M. J Am Chem Soc 1997, 119, 4239.
35. Valgimigli, L.; Banks, J. T.; Ingold, K. U.; Lusztyk, J. J Am Chem Soc 1995, 117, 9966.
36. Li, X.-Y.; Liu, J.-F. J Comput Chem 2001, 22, 1067.
37. Cheng, Y.-M.; Pu, S.-C.; Hsu, C.-J.; Lai, C.-H.; Chou, P.-T. Chem Phys Chem 2006, 7, 1372.
38. Muchová, E.; Špirko, V.; Hobza, P.; Nachtigallová, D. Phys Chem Chem Phys 2006, 8, 4866.
39. Mikami, N.; Okabe, A.; Suzuki, I. J Phys Chem 1988, 92, 1858.
40. Steadman, J.; Syage, J. A. J Chem Phys 1990, 92, 4630.
41. Syage, J. A.; Steadman, J. J Chem Phys 1991, 95, 2497.
42. Steadman, J.; Syage, J. A. J Am Chem Soc 1991, 113, 6786.
43. Syage, J. A.; Steadman, J. J Phys Chem 1992, 96, 9606.
44. Mikami, N.; Sato, S.; Ishigaki, M. Chem Phys Lett 1993, 202, 431.
45. Yi, M.; Scheiner, S. Chem Phys Lett 1996, 262, 567.
46. Sodupe, M.; Oliva, A.; Bertrán, J. J Phys Chem A 1997, 101, 9142.
47. Vener, M. V.; Iwata, S. Chem Phys Lett 1998, 292, 87.
48. Martrenchard-Barra, S.; Dedonder-Lardeux, C.; Jouvet, C.; Solgadi, D.; Vervloet, M.; Gregoire, G.; Dimicoli, I. Chem Phys Lett 1999, 310, 173.
49. Pino, G.; Dedonder-Lardeux, C.; Gregoire, G.; Jouvet, C.; Martrenchard, S.; Solgadi, D. J Chem Phys 1999, 111, 10747.
50. Kim, H.-T.; Green, R. J.; Qian, J.; Anderson, S. L. J Chem Phys 2000, 112, 5717.
51. David, O.; Dedonder-Lardeux, C.; Jouvet, C. Int Rev Phys Chem 2002, 21, 499.
52. Domcke, W.; Sobolewski, A. L. Science 2003, 302, 1693.
53. Qin, Y.; Wheeler, R. A. J Chem Phys 1995, 102, 1689.
54. Adamo, C.; Barone, V. In Recent Development in Density Functional Methods; Chong, D. P., Ed.; World Scientific Publishing: Singapore, 1997; Part II.
55. O'Malley, P. J. J Phys Chem A 1997, 101, 6334.
56. Kim, S. K.; Bok, J. H.; Bartsch, R. A.; Lee, J. Y.; Kim, J. S. Org Lett 2005, 7, 4839.
57. Yan, S.; Bu, Y. J Chem Phys 2005, 122, 184324.
58. Yan, S.; Zhang, L.; Cukier, R. I.; Bu, Y. Chem Phys Chem 2007, 8, 944.
59. Frisch, M. J.; Trucks, G. W.; Schlegel, H. B.; Scuseria, G. E.; Robb, M. A.; Cheeseman, J. R.; Montgomery, Jr., J. A.; Vreven, T.; Kudin, K. N.; Burant, J. C.; Millam, J. M.; Iyengar, S. S.; Tomasi, J.; Barone, V.; Mennucci, B.; Cossi, M.; Scalmani, G.; Rega, N.; Petersson, G. A.; Nakatsuji, H.; Hada, M.; Ehara, M.; Toyota, K.; Fukuda, R.; Hasegawa, J.; Ishida, M.; Nakajima, T.; Honda, Y.; Kitao, O.; Nakai, H.; Klene, M.; Li, X.; Knox, J. E.; Hratchian, H. P.; Cross, J. B.; Bakken, V.; Adamo, C.; Jaramillo, J.; Gomperts, R.; Stratmann, R. E.; Yazyev, O.; Austin, A. J.; Cammi, R.; Pomelli, C.; Ochterski, J. W.; Ayala, P. Y.; Morokuma, K.; Voth, G. A.; Salvador, P.; Dannenberg, J. J.; Zakrzewski, V. G.; Dapprich, S.; Daniels, A. D.; Strain, M. C.; Farkas, O.; Malick, D. K.; Rabuck, A. D.; Raghavachari, K.; Foresman, J. B.; Ortiz, J. V.; Cui, Q.; Baboul, A. G.; Clifford, S.; Cioslowski, J.; Stefanov, B. B.; Liu, G.; Liashenko, A.; Piskorz, P.; Komaromi, I.; Martin, R. L.; Fox, D. J.; Keith, T.; Al-Laham, M. A.; Peng, C. Y.; Nanayakkara, A.; Challacombe, M.; Gill, P. M. W.; Johnson, B.; Chen, W.; Wong, M. W.; Gonzalez, C.; Pople, J. A. Gaussian 03, Revision D.02; Gaussian Inc.: Wallingford, CT, 2004.

60. Reed, A. E.; Curtiss, L. A.; Weinhold, F. Chem Rev 1998, 88, 899–926.
61. Miertus, S.; Scrocco, E.; Tomsi, J. Chem Phys 1981, 55, 117.
62. Miertus, S.; Tomsi, J. Chem Phys 1982, 65, 239.
63. Cossi, M.; Barone, V.; Cammi, R. Tomasi, J. Chem Phys Lett 1996, 255, 327.
64. Cammi, R. J Chem Phys 1998, 109, 3185.
65. Cammi, R.; Mennucci, B.; Tomasi, J. J Am Chem Soc 1998, 120, 8834.
66. Cammi, R.; Mennucci, B.; Tomasi, J. J Phys Chem A 1998, 102, 870.
67. Cammi, R.; Mennucci, B.; Tomasi, J. J Phys Chem A 2001, 105, 7287.
68. Daigoku, K.; Ishiuchi, S.; Sakai, M.; Fujii, M.; Hashimoto, K. J Chem Phys 2003, 119, 5149.
69. Ishiuchi, K.; Daigoku, K.; Saeki, M.; Sakai, M.; Hashimoto, K.; Fujii, M. J Chem Phys 2002, 117, 7083.
70. Gerlt, J. A.; Gassman, P. G. J Am Chem Soc 1993, 115, 11552.
71. Gerlt, J. A.; Gassman, P. G. Biochemistry 1993, 32, 11943.
72. Cleland, W. W.; Kreevoy, M. M. Science 1994, 264, 1887.
73. Frey, P. A.; Whitt, S. A.; Tobin, J. B. Science 1994, 264, 1927.
74. Warshel, A.; Papazyan, A.; Kollman, P. A.; Cleland, W. W.; Kreevoy, M. M.; Frey, P. A. Science 1995, 269, 102.
75. Tobin, J. B.; Whitt, S. A.; Cassidy, C. S.; Frey, P. A. Biochemistry 1995, 34, 6919.
76. Shan, S.-O.; Loh, S.; Herschlag, D. Science 1996, 272, 97.
77. Kim, K. S.; Oh, K. S.; Lee, J. Y. Proc Natl Acad Sci USA 2000, 97, 6373.
78. Kim, K. S.; Kim, D.; Lee, J. Y.; Tarakeshwar, P.; Oh, K. S. Biochemistry 2002, 41, 5300.
79. Chen, J.; McAllister, M. A.; Lee, J. K.; Houk, K. N. J Org Chem 1998, 63, 4611.
80. Alabugin, I. V.; Manoharan, M.; Peabody, S.; Weinhold, F. J Am Chem Soc 2003, 125, 5973.
81. Sychrovský, V.; Šponer, J.; Hobza, P. J Am Chem Soc 2004, 126, 663–672.
82. Gonohe, N.; Abe, H.; Mikami, N. J Phys Chem 1985, 89, 3642.
83. Mikami, N.; Suzuki, I.; Okabe, A. J Phys Chem 1987, 91, 5242.
84. Stranzl, G. R.; Gruber, K.; Steinkellner, G.; Zangger, K.; Schwab, H.; Kratky, C. J Biol Chem 2004, 279, 3699.
85. Perrin, C. L.; Nielson, J. B. Annu Rev Phys Chem 1997, 48, 511.
86. Kumar, G. A.; Pan, Y.; Smallwood, C. J.; McAllister, M. A. J Comput Chem 1998, 19, 1345.
87. Li, G.-S.; Maigret, B.; Rinaldi, D.; Ruiz-López, M. F. J Comput Chem 1998, 19, 1675.
88. Pacios, L. F.; Gómez, P. C.; Gálvez, O. J Comput Chem 2006, 27, 1650.